Modeling Catalytic Effects of Clay Mineral Surfaces on Peptide Bond Formation

Adélia J. A. Aquino,*,†,‡ Daniel Tunega,†,‡ Martin H. Gerzabek,§ and Hans Lischka*,†

Institute for Theoretical Chemistry and Structural Biology, University of Vienna, Währingerstrasse 17, A-1090 Vienna, Austria, Austrian Research Centers Seibersdorf, A-2444 Seibersdorf, Austria, and Institute of Soil Research, University of Agricultural Sciences, Gregor-Mendel Strasse 33, A-1180 Vienna, Austria

Received: February 25, 2004; In Final Form: April 28, 2004

The catalysis of the amide-bond formation for the concerted reaction of acetic acid and methylamine on clay mineral surfaces has been studied by means of density functional theory calculations. Two typical cluster models for surface defects representing hydrogen-bonded interactions (physical defect) and a Lewis acid (chemical) defect have been selected. Additionally, a series of catalysts of varying strength (Al^{3+}, $AlCl_3$, $Al(OH)_3$, $[Al(H_2O)_5]^{3+}$, H^+, H_3O^+, $H_3O^+-H_2O$, H_2O, and $(H_2O)_2$), which can act as Lewis or Brønsted acids was investigated as well. Reaction energies, activation barriers and corresponding thermodynamic quantities have been calculated. The results show a strongly asynchronous mechanism with the prior formation of a N−C dative bond followed by a proton transfer from nitrogen to oxygen as the rate-determining step. The barrier height was reduced substantially by the interaction with the catalyst. Solvation effects were taken into account by explicit inclusion of water molecules and by the polarizable continuum solvation model (PCM).

I. Introduction

The relevance of the catalysis of peptide formation on surfaces of natural aluminosilicates in the context of pre-biological chemical evolution was suggested for the first time by Bernal.[1] Numerous attempts were performed to prepare simple peptides under conditions resembling natural conditions in primitive prebiotic times of the earth.[1−3] For example, it was found that the presence of divalent cations (e.g., Mg^{2+}, Cu^{2+}, or Zn^{2+}) can enhance the formation of peptides[4−7] leading to the Salt-Induced Peptide Formation (SIPF) reaction model. Clay minerals such as kaolinites or smectites were tested also for their catalytic capabilities concerning the synthesis of peptides from simple amino acids.[8−10] These experiments showed that peptides were formed in the presence of clays, albeit relatively small yields were reached. In recent experiments[11−14] various forms of alumina were used under different acid/base conditions, and higher yields than in case of clay minerals were obtained. The higher catalytic efficiency of alumina was assigned to its enhanced defect surface structure. Despite the intensive experimental work on the use of clays and alumina as catalysts for the peptide formation, mechanistic discussions are rare and no detailed molecular picture is available for these processes.

The mechanism of the peptide bond formation has been studied experimentally for the acid/base-catalyzed aminolysis of alkyl esters in aqueous solution by Jencks and coworkers.[15−17] The basic step is the nucleophilic attack of the lone electron pair of the amino group onto the carbon atom of the carboxyl group followed by proton transfer from the amino group to one of the oxygen atoms of the carboxyl group. In the proposed concerted and/or stepwise reaction mechanisms a possible formation of a relatively stable zwitterionic intermediate $T^{\pm}$is considered. The relative stability of this adduct depends on the acido-base properties of the solvent, and its lifetime can be an important factor in the whole reaction mechanism.

Concerted and stepwise reaction mechanisms of the peptide bond formation were studied theoretically by Oie et al.,[18−20] Jensen et al.,[21] and Chalmet et al.[22] The theoretical calculations for the uncatalyzed reaction in the gas phase showed that both reaction mechanisms, stepwise and concerted, can coexist since both of them have similar activation energies of about 35−40 kcal/mol. From a comparison of results obtained for the reaction of two glycine molecules and those of the prototype reaction ammonia plus formic acid, it was concluded that the latter reaction provided already a good model for the peptide formation.[21] Later on, solvent effects were taken into account by Chalmet et al.[22] in self-consistent reaction field (SCRF) and quantum chemical/molecular mechanics (QM/MM) calculations, which were performed for the system ammonia plus formic acid.

The reverse problem to the amide-bond formation, the amide-bond hydrolysis, was studied in several theoretical investigations also. Antonczak et al.[23] investigated the water-assisted, H_3O^+-promoted hydrolysis of formamide, while Bakovies and Kollman[24] studied the same problem in basic environment. A detailed analysis of the chemical bonding in the course of the neutral, acid- and base-promoted hydrolysis based on the Laplacian of the charge density has been given by Krug et al.[25]

Catalytic effects have been considered under several points of view. For example, the role of amine catalysis[19] and the effect of divalent cations[20,26] have been investigated. These theoretical studies showed significant lowering of the reaction barriers. In the case of amine catalysis an additional amine molecule functioning as mediator facilitates the proton transfer from the amino group to the carboxyl group. The role of the divalent cations is a different one. In this case a chelate ring is formed involving the oxygen of the carbonyl group. The proton transfer is not affected directly by any bridging molecule. The two catalytic alternatives have been combined in studies of a H_3O^+-

* Authors to whom correspondence should be addressed. E-mail: adelia.aquino@univie.ac.at; hans.lischka@univie.ac.at.
† University of Vienna.
‡ Austrian Research Centers Seibersdorf.
§ University of Agricultural Sciences.

10.1021/jp049149d CCC: $27.50
Published on Web 06/15/2004

SCHEME 1

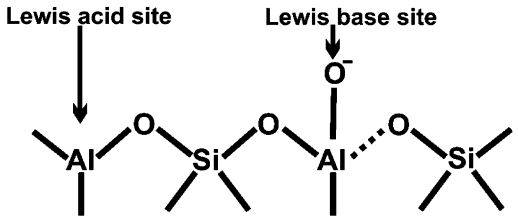

SCHEME 2

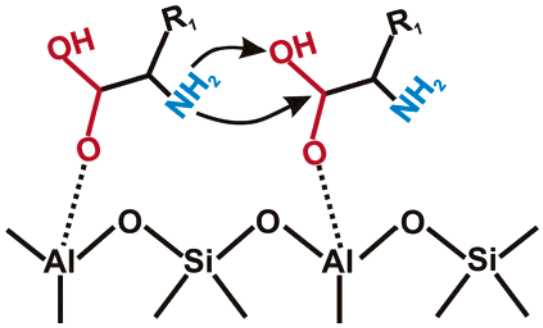

promoted, water-assisted amide hydrolysis by Antonczak et al.[23] A comparison of the different catalysis modes shows that the H_3O^+ promotion is far more effective as compared to the water-assisted case without promotion. Most effective is the aforementioned combined mode.

All these theoretical investigations on the formation of the peptide bond have been performed with the focus on the homogeneous, aqueous solution. Also the experimental investigations by Jencks and co-workers[15−17] were performed under the same conditions. The catalytic role of minerals on peptide bonding has not been studied yet experimentally in the same detail. The situation is much more difficult under these circumstances. Mainly global effects of peptide yields and environmental conditions have been investigated. The situation encountered here differs from the acid/base catalysis described above in several aspects. One of them is the fact that, in addition to Brønsted acids or bases, Lewis acids and bases also play an important role. It is the aim of the present work to investigate systematically the effect of selected defect models for clay surfaces with respect to their ability to reduce the activation barrier for the amide bond formation. A general picture of possible active centers on mineral surfaces is given in Scheme 1.

In this scheme, an aluminum atom which had lost its hydroxyl group acts as an electrophilic (Lewis acid) defect. Additionally, depending on the pH, also O^-, OH, or OH_2^+ defects can occur on the mineral surfaces.[27] Especially O^-, as a strong Lewis base site, could be important in the reaction of the peptide bond formation. Sites such as OH or OH_2^+ are also able to assist in adsorption of molecular species, for example, via hydrogen bonds. Following the ideas of Bujdak et al.,[11,12] one main feature of the interaction of the amino acid with the clay defects will be the bond between the electrophilic aluminum and the oxygen of the carbonyl group of the amino acid. Further hydrogen-bonded interactions will lead to specific orientations of the amino acid on the surface, depending on the distribution of individual defects. A possible orientation of two amino acids on the clay surface with the possibility to form a peptide bond is depicted in Scheme 2.

The interaction of the carbonyl oxygen with the aluminum defect resembles the cases of H_3O^+ promotion and interaction with divalent cations discussed before. The partial negative charge located at the carbonyl oxygen is stabilized by the interaction with the electrophilic aluminum. Additionally, the C═O bond is polarized toward the oxygen atom, leading to an increase of positive charge on the carbon atom. This latter fact should facilitate the nucleophilic attack of the nitrogen on this carbon atom and reduce the activation barrier for the amide bond formation.

As has already been mentioned, the relatively simple reaction of ammonia and formic acid already constitutes a good model for the formation of peptide bonds.[18] Our starting point is a slightly more complex system, the reaction between methylamine and acetic acid, which is displayed in Scheme 3.

It consists of the acetic acid (HAc) with the carbonyl oxygen attached to the surface defect in analogy to Scheme 2 and reacting with methylamine (MA). In view of the fact that the formation of the amide bond is a bimolecular reaction, a pre-reaction complex (either intermolecular complex or a zwitterionic structure) is included in the reaction Scheme 3. This pre-reaction complex corresponds practically to the reaction intermediate $T^{\pm}$ considered in the experimental investigations.[15−17] Therefore, the label $T^{\pm}$ will be used for it. The reaction pathway for the peptide-bond formation leads from the pre-reaction complex to the transition structure, which can decay to NMA and H_2O. The concerted reaction mechanism was investigated only since the carbonyl group, which is activated in the stepwise mechanism, is blocked in the proposed adsorption model.

The calculations had to be performed at a quantum chemical level in order to allow a proper description of the chemical reaction. The density functional theory (DFT) method was chosen finally because of its computational efficiency. In such calculations the use of larger segments of the clay surface would still have been a very time-consuming task even with present computer facilities. Such extended investigations have been performed, e.g., in our group on simpler problems such as the adsorption processes of selected molecules (e.g., water, acetic acid, herbicides derived from the phenoxyacetic acid) on regular kaolinite surfaces[28,29] using Car-Parinello-type[30] calculations with the Vienna Ab Initio Simulation Package (VASP).[31,32] On the other hand, smaller and therefore much less time-consuming cluster models have been used quite successfully for studying adsorption processes on clay mineral surfaces.[33−38] In particular,

SCHEME 3

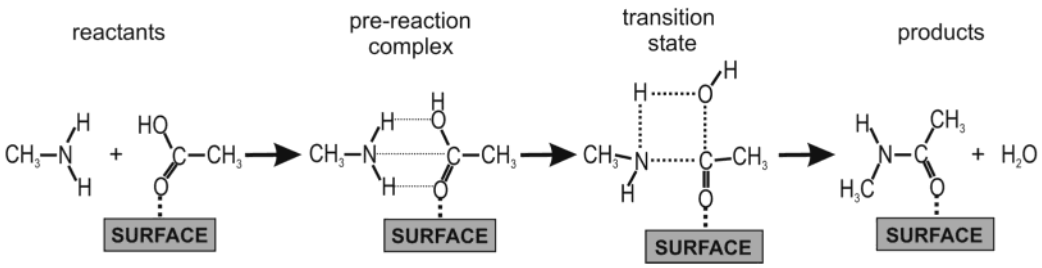

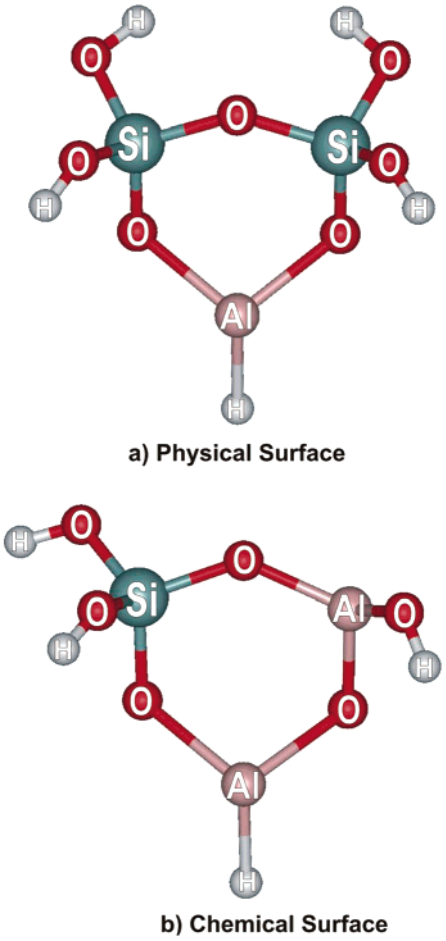

Figure 1. Cluster models of broken surfaces of phyllosilicate structures: (a) surface terminated with hydroxyl groups, (b) defect surface with Al substitution for Si.

we want to mention our own previous study on the interaction of acetic acid and *N*-methylacetamide (NMA) with various surface defect sites.[38] In the present work we use the model clusters developed in our previous investigation for the description of a physical (hydrogen-bonded) and chemical (Lewis acid type) defect site (see Figure 1). Additionally, we used a series of model catalysts (CA = Al^{3+}, $AlCl_3$, $Al(OH)_3$, $[Al(H_2O)_5]^{3+}$, H^+, H_3O^+, $H_3O^+-H_2O$, H_2O, and $(H_2O)_2$), which can act as Lewis or Brønsted acids to stabilize the partial negative charge at the carbonyl oxygen, or can interact via hydrogen bonds. These species were selected in order to create a scale of interactions of different strength, which could be compared with the two defect site models. The first part of the list contains the bare Al^{3+} cation as an extreme example of a Lewis acid, two aluminum compounds with Lewis activity and the aluminum pentaaquo complex, in which the sixth coordination is used for the interaction with the carbonyl oxygen. We have added to our set also the proton although amines are protonated in the acidic environment, a fact which inhibits nitrogen attack on the carbon atom of the −COOH group.[39] The proton, H_3O^+, and $H_3O^+-H_2O$ comprise the second part of the list. The third group of CA contains neutral water and the water dimer.

II. Structural and Computational Details

The two clusters, which were used to simulate a broken surface of phyllosilicates are displayed in Figure 1. In the first model (see Figure 1a), which has the chemical formula $Si_2AlO_5H_3(OH)_2$, two connected SiO_4 tetrahedra represent part of the tetrahedral sheet of a single layer in phyllosilicate minerals ended with two terminal hydroxyl groups as possible interaction sites. The other two OH groups are considered as part of the solid bulk since they originate from saturation of dangling bonds. This model is labeled physical surface (PhS) since both terminal surface hydroxyl groups can act in physical sorption via hydrogen bonds. In the second model (chemical formula $SiAl_2O_5H_3OH$), depicted in Figure 1b, one silicon atom in the tetrahedral position was replaced by aluminum and one terminal hydroxyl anion bound to this tetrahedral site was removed to balance the charge. The aluminum in the tetrahedral sheet is considered as an active site for chemical sorption. Thus, this model was labeled as chemical surface (ChS). In both models, an additional aluminum atom represents part of the octahedral sheet of the phyllosilicate layer and is terminated with H^- in order to conserve charge neutrality of both models. For more information on other termination options see ref 38. Additionally, several molecular species of different chemical nature as listed in the Introduction were selected as possible catalysts.

All calculations were performed with the Gaussian98 package.[40] The B3LYP[41] method and the triple-ζ-valence polarized (TZVP) basis set by Ahlrichs and co-workers[42] were selected as key combination in our study. With the exception of the surface fragments (PhS, ChS) full geometry optimizations, transition-state searches and frequency calculations were performed at the default conditions adjusted in Gaussian98. In the case of the model PhS and ChS surfaces, the geometry optimization and the transition-state calculations were performed with a partly frozen structure in order to maintain the basic features (distances, angles) of the phyllosilicate surface. The nature and quality of the stationary points were controlled by calculations of Hessians and corresponding vibrational frequencies. Each transition state reported below was a saddle point of first order and it was tested whether the negative frequency corresponded to the reaction center. Specific cases where a transition state was not obtained are discussed in the next section. In several cases, intrinsic reaction coordinates (IRC)[43,44] for the reaction paths were calculated connecting the transition state with the corresponding minima. For all stationary points, zero-point energies, enthalpies, and Gibbs free energies at 298 K were calculated within the harmonic oscillator-rigid rotor approximation. Atomic charges were computed from the natural population analysis (NPA).[45]

For verification of the B3LYP/TZVP accuracy, the Møller−Plesset perturbation theory to second order (MP2)[46−48] was used. For the catalyzed reactions, the MP2/TZVP calculations were performed at the MP2 geometries using the SVP basis.[49] For the uncatalyzed case, full MP2/TZVP geometry optimizations were performed. The set of methodological tests was completed by single-point B3LYP/TZVPP calculations (TZVP basis set augmented by additional polarization functions) at the B3LYP/TZVP geometry of reactants and products. The effect of a solvent environment on the formation of the peptide bond was studied using the Polarized Continuum Model (PCM).[50−52] The calculations for the liquid phase were carried out using water as solvent with the relative dielectric constant $\epsilon_r = 78.39$. The optimized structures obtained in the calculations in the gas phase for reactants, products, and transition states were used as starting point in the calculations in the water solvent. In some cases the geometry convergence using PCM was not reached, so only the single-point calculations on the gas-phase optimized geometries were performed. The PCM model is meant to take into account global solvation effects. Specific effects of individual water molecules were included in those cases where water acted

TABLE 1: Reaction Energies ΔE_r and Thermodynamic Data for the Gas Phase (kcal/mol) Obtained with Different Methods and Basis Sets

		MP2/SVP	MP2/TZVP[a]	B3LYP/SVP	B3LYP/TZVP			B3LYP/TZVPP[b]
reactants	products	ΔE_r	ΔE_r	ΔE_r	ΔE_r	ΔH_r	ΔG_r	ΔE_r
HAc + MeA	NMA + H_2O	−2.5	−4.2	−0.2	−3.0	−3.7	−3.7	−3.1
HAc···H_2O + MeA	NMA···H_2O + H_2O	1.6	−1.1	4.7	0.4	−0.4	−2.4	0.9
HAc···$2H_2O$ + MeA	NMA···$2H_2O$ + H_2O	3.6	−0.6	8.2	3.1	2.6	1.3	2.3
HAc···PhS + MeA	NMA···PhS + H_2O	−1.1	−5.1	1.3	−3.0	−	−	−2.8
HAc···ChS + MeA	NMA···ChS + H_2O	−9.4	−11.9	−5.9	−9.1	−	−	−8.8
HAc···$AlCl_3$ + MeA	NMA···$AlCl_3$ + H_2O	−8.0	−11.8	−4.9	−7.0	−6.5	−7.7	−6.5
HAc···$Al(OH)_3$ + MeA	NMA···$Al(OH)_3$ + H_2O	−9.4	−10.6	−6.3	−8.4	−8.8	−8.3	−8.3
HAc···H^+ + MeA	NMA···H^+ + H_2O	−33.5	−36.2	−29.2	−33.2	−33.6	−31.7	−32.3
HAc···H_3O^+ + MeA	NMA···H_3O^+ + H_2O	−23.2	−26.2	−19.0	−23.3	−23.1	−23.0	−22.6
HAc···(H_3O^+−H_2O) + MeA	NMA ···(H_3O^+−H_2O) +H_2O	−15.1	−23.4	−14.5	−20.4	−21.7	−20.4	−20.1
HAc···Al^{3+} + MeA	NMA···Al^{3+} + H_2O	−94.4	−98.0	−75.2	−81.5	−81.7	−80.7	−77.6
HAc···$[Al(H_2O)_5]^{3+}$ + MeA	NMA···$[Al(H_2O)_5]^{3+}$ + H_2O	−24.1	−26.1	−19.1	−22.4	−22.5	−23.9	−23.7

[a] Single-point calculations at the MP2/SVP geometry. [b] Single-point calculations at the B3LYP/TZVP geometry.

as catalyst interacting with the carbonyl oxygen. Water-assisted processes as they were investigated, e.g., in the work of Antonczak et al.,[23] were not taken into account. Micro-solvation of surface hydroxyl groups with explicit inclusion of one and two water molecules has been investigated by us previously and used for the description of the competitive adsorption between water and acetic acid.[38] It was found that the energetic balance of this competition was fairly close and depended on the details of the model. More extended, but also much more time-consuming models need to be used in order to obtain a more realistic description of the micro-solvation and competitive adsorption. The computed close energetic balance is in correspondence with the experimental observation of the absence of significant adsorption of HAc on clays.[53]

The calculated reaction or activation energies refer to the reaction scheme given in Scheme 3. The activation energy $\Delta E^{\#}_{fw}$ (and the corresponding activation enthalpy and activation Gibbs free energy) for the forward reaction was calculated with respect to the pre-reaction complex as

$$\Delta E^{\#}_{fw} = E(\mathrm{TS}\cdots\mathrm{CA}) - E(\mathrm{T}^{\pm}\cdots\mathrm{CA}) \quad (1)$$

The stabilization energy ΔE_c, of the pre-reaction complex formation is defined with respect to the isolated products

$$\Delta E_c = E(\mathrm{T}^{\pm}\cdots\mathrm{CA}) - E(\mathrm{HAc}\cdots\mathrm{CA}) - E(\mathrm{MA}) \quad (2)$$

and the reaction energy ΔE_r is computed as

$$\Delta E_r = E(\mathrm{NMA}\cdots\mathrm{CA}) + E(\mathrm{H_2O}) - E(\mathrm{HAc}\cdots\mathrm{CA}) - E(\mathrm{MA}) \quad (3)$$

For the fully optimized models reaction/stabilization enthalpies (ΔH_r and ΔH_c) and Gibbs free energies (ΔG_r and ΔG_c) were calculated too. The activation energy with respect to the isolated reactants and/or products will be presented also. The term overall activation barrier for

$$\Delta E^{\#}_{of} = E(\mathrm{TS}\cdots\mathrm{CA}) - E(\mathrm{HAc}\cdots\mathrm{CA}) - E(\mathrm{MA}) \quad (4)$$

will be used to distinguish it from the one computed with respect to the pre-reaction complex. The overall activation energy can also be calculated as the sum of the complexation energy ΔE_c and the activation energy $\Delta E^{\#}_{fw}$:

$$\Delta E^{\#}_{of} = \Delta E^{\#}_{fw} + \Delta E_c \quad (5)$$

TABLE 2: Overall Activation Barriers $\Delta E^{\#}_{of}$, Reaction Energies ΔE_r with Respect to the Isolated Reactants and/or Products, Respectively, Thermodynamic Data and Geometry Parameters of the C−O−H−N Reaction Center for the Uncatalyzed Reaction[a]

	B3LYP/SVP	B3LYP/TZVP	MP2/SVP	MP2/TZVP
ΔE_r	−0.2	−3.0	−2.5	−4.6
ΔH_r	−0.9	−4.3	−3.3	−5.5
ΔG_r	−1.0	−3.7	−2.6	−5.1
$\Delta E^{\#}_{of}$	37.0	38.7	36.0	34.6
$\Delta H^{\#}_{of}$	35.1	37.1	33.9	32.7
$\Delta G^{\#}_{of}$	48.0	49.8	46.6	45.8
C−O	1.861	1.969	1.832	1.914
O−H	1.345	1.417	1.329	1.317
H−N	1.178	1.132	1.180	1.186
N−C	1.622	1.609	1.603	1.587
∠(N−C−O)	81.9	79.9	92.7	81.0
∠(C−O−H)	67.1	64.9	67.3	65.8
∠(O−H−N)	130.2	130.0	130.1	132.0
∠(H−N−C)	79.6	84.4	79.0	80.9

[a] Energies are in kcal/mol, distances in Å, and angles in degrees.

Complete geometries for all structures investigated in this work computed at the B3LYP/TZVP level are available as Supporting Information (see the end of the text for more information).

III. Results and Discussion

3.1. Comparison of MP2 and DFT Results. In this section, results obtained with the MP2 and B3LYP methods using several basis sets are compared in order to give support to the final use of the B3LYP method. These tests have been performed for the reaction energy of the uncatalyzed and catalyzed cases (see Table 1) and for the activation barrier of the uncatalyzed reaction (Table 2). MP2 and B3LYP results, shown in Table 1, usually differ by about 1−3 kcal/mol for a given basis. Agreement between the two methods is in most cases better at the TZVP basis than at the SVP basis. One exception is the interaction with the Al^{3+} cation where the difference between MP2/TZVP and B3LYP/TZVP is much larger. Inspection of the optimized structures of reactants and products clarified this big difference. A structure with the dihedral angle of the −79° value for the C−N−C−C backbone in the NMA···Al^{3+} complex was obtained at the MP2/SVP level differing significantly from the value of −17° obtained with B3LYP/TZVP calculations. The last column in Table 1 presents B3LYP/TZVPP//B3LYP/TZVP results. Comparison with the B3LYP/TZVP energies showed that augmentation of the TZVP

TABLE 3: Selected Structural Parameters, NPA Charges on HAc and Total Charge Transfer CT for HAc···CA Complexes Computed at the B3LYP/TZVP Level[a]

system	C═O	C−OH	∠O═C−OH	q(C)	$-q(O_{carb})$	$-q(O_{OH})$	$-q$(OH)	CT[b]
HAc	1.204	1.359	122.5	0.744	0.563	0.663	0.180	0.0000
HAc···H_2O	1.217	1.338	123.3	0.867	0.661	0.725	0.217	−0.0196
HAc···$2H_2O$	1.221	1.325	124.4	0.770	0.665	0.726	0.152	−0.0286
HAc···PhS	1.221	1.334	123.2	0.772	0.648	0.654	0.143	−0.0092
HAc···ChS	1.237	1.321	118.9	0.832	0.669	0.598	0.101	0.1421
HAc···$AlCl_3$	1.247	1.300	123.4	0.832	0.709	0.596	0.093	0.0970
HAc···$Al(OH)_3$	1.233	1.324	119.2	0.828	0.664	0.605	0.109	0.1236
HAc···H^+	1.285	1.285	124.1	0.971	0.587	0.588	0.060	0.4723
HAc···H_3O^+	1.266	1.290	117.9	0.951	0.636	0.602	0.075	0.3374
HAc···H_3O^+−H_2O	1.267	1.288	124.4	0.835	0.560	0.583	0.062	0.3231
HAc···Al^{3+}	1.369	1.230	126.8	0.908	0.934	0.418	0.185	0.6960
HAc···$[Al(H_2O)_5]^{3+}$	1.259	1.314	115.4	0.873	0.750	0.627	0.073	0.2087

[a] Distances are in Å, angles in degrees and charges in $|e|$. [b] Charge transfer from HAc to CA.

basis set with additional polarization functions brought only small changes. Relatively small changes in basis set and methods were also observed for overall activation energies and respective thermodynamic data for the uncatalyzed reaction as presented in Table 2. Structural parameters describing the reaction center are given also. The comparison of activation energies, enthalpies, and Gibbs free energies shows again larger deviations with respect to the basis set than for different methods. The largest variation in the geometry of the transition state (about 0.1 Å) for a given method is observed for the C−O bond. The O−H bond distance is also quite sensitive to the selected computational method. However, one should keep in mind that these are strongly stretched bonds far away from equilibrium values of the original reactants. Therefore, larger variations with basis set and method can occur than in case of equilibrium bond lengths. Practically negligible differences among all tested methods are observed for the four angles within the reaction center. It is noted that the reaction center is not entirely planar. However, the deviation is small with about 8°. Similar or even smaller deviations from planarity were also found for the remaining transition states including the catalysts. Comparison with the results obtained by Jensen et al.[21] and by Chalmet et al.[22] for the similar reaction ammonia + formic acid → formamide + water shows quite reasonable agreement in terms of the geometry of the four-center transition structure and the reaction and activation energies. The results presented in Tables 1 and 2 demonstrate the importance of the selection of the proper basis set especially for the transition structures. The B3LYP/TZVP approach was found to be an economic and quite reliable choice and, therefore, was selected for further calculations.

3.2. The HAc···CA Complexes. The global characteristic of the HAc···CA structures is similar to the saddle-point structures of the corresponding catalyst (see Figure 2). Therefore, these structures are not given separately. From inspection of Figure 2, one can see that several catalysts interact with HAc only via its carbonyl oxygen. This is the case for PhS, ChS, $AlCl_3$, H_3O^+, H^+, and Al^{3+}. In the other examples, water molecules are involved (H_2O, $(H_2O)_2$, $H_3O^+(H_2O)$), which form additional hydrogen-bonded interactions with the OH group of HAc. The same is also true for $Al(OH)_3$. It should be mentioned that in case of the interactions with H_3O^+ and $H_3O^+(H_2O)$, respectively, proton transfer from H_3O^+ to the carbonyl oxygen has taken place. A protonated HAc molecule is formed with two almost equal C−O bonds (see Table 3). The water molecule released after the H_3O^+ decay remained in its position in order to form hydrogen bonds with the protonized HAc molecule. A similar effect has already been found by Antonczak et al.[23]

Structural data describing the carboxyl group are given in Table 3 together with NPA charges and total charge transfer CT from HAc to the catalyst. The data collected in Table 3 are analyzed graphically in Figure 3 in terms of correlations between atomic charges/total charge transfer and the C═O bond length. The polarization of the C═O bond is illustrated nicely in Figure 3a by the increase (in absolute value) of the atomic charges of the carbon and carbonyl oxygen (O_{carb}) atoms with lengthening of the C═O bond. The changes are largest for $q(O_{carb})$ since it is directly connected to the polarizing catalyst. The three $q(O_{carb})$ cases deviating from the general trend shown in Figure 3a belong to H^+, H_3O^+, and $H_3O^+(H_2O)$. In all of these three cases the proton is directly bound to the carbonyl oxygen and, as a consequence, the charge was transferred on from the carbonyl oxygen to the proton. This can also be seen from the large total charge transfer in these cases. The increase of the positive charge of the C atom with increasing strength of the catalyst signifies an increased charge deficiency on this atom and, thus, facilitates nucleophilic attack by the lone pair of the amine.

The total charge-transfer correlates very well with the elongation of the C═O bond (see Figure 3b). The amount of total charge transfer depends on the catalyst and its ability to bind to the HAc molecule. The different catalysts can be separated into several groups. To the first one belong the water molecules and the physical surface. In these cases HAc forms hydrogen bonds with water and the surface hydroxyl groups, respectively. A small charge transfer (from the catalysts to the HAc molecule) is observed. The neutral species of Lewis acid-type, $AlCl_3$, $Al(OH)_3$, and ChS, belong to the second group of catalysts where charge-transfer complexes arise in which the carboxyl group is in contact with the Lewis acid center represented by the aluminum atom. The charge redistribution within the HAc molecule and the polarization of the C═O group is significantly stronger than in the previous case of the hydrogen-bonded complexes. The last group of catalysts is represented by the positively charged species. Very strong charge-transfer complexes are created and a large charge transfer from the HAc molecule to the charged compound is observed. The Al^{3+} cation exerts the strongest effects. In this extreme case the C−OH bond is even shorter than the C−O bond. The Al^{3+} cation represents a super strong Lewis acid and the largest amount of the charge transfer is observed (see Table 3). In solution the free Al^{3+} cation is, of course, not observed. Therefore, the interaction of the HAc molecule with the pentaaqua aluminum complex was investigated where the carboxyl group is occupying the sixth coordination position of Al^{3+}. The bond lengths and the CT are similar to the cases containing the H_3O^+ cation.

3.3. The Pre-reaction Complexes. The pre-reaction complexes were obtained from the optimized transition state by separating the MA and HAc molecules to a C−N distance of

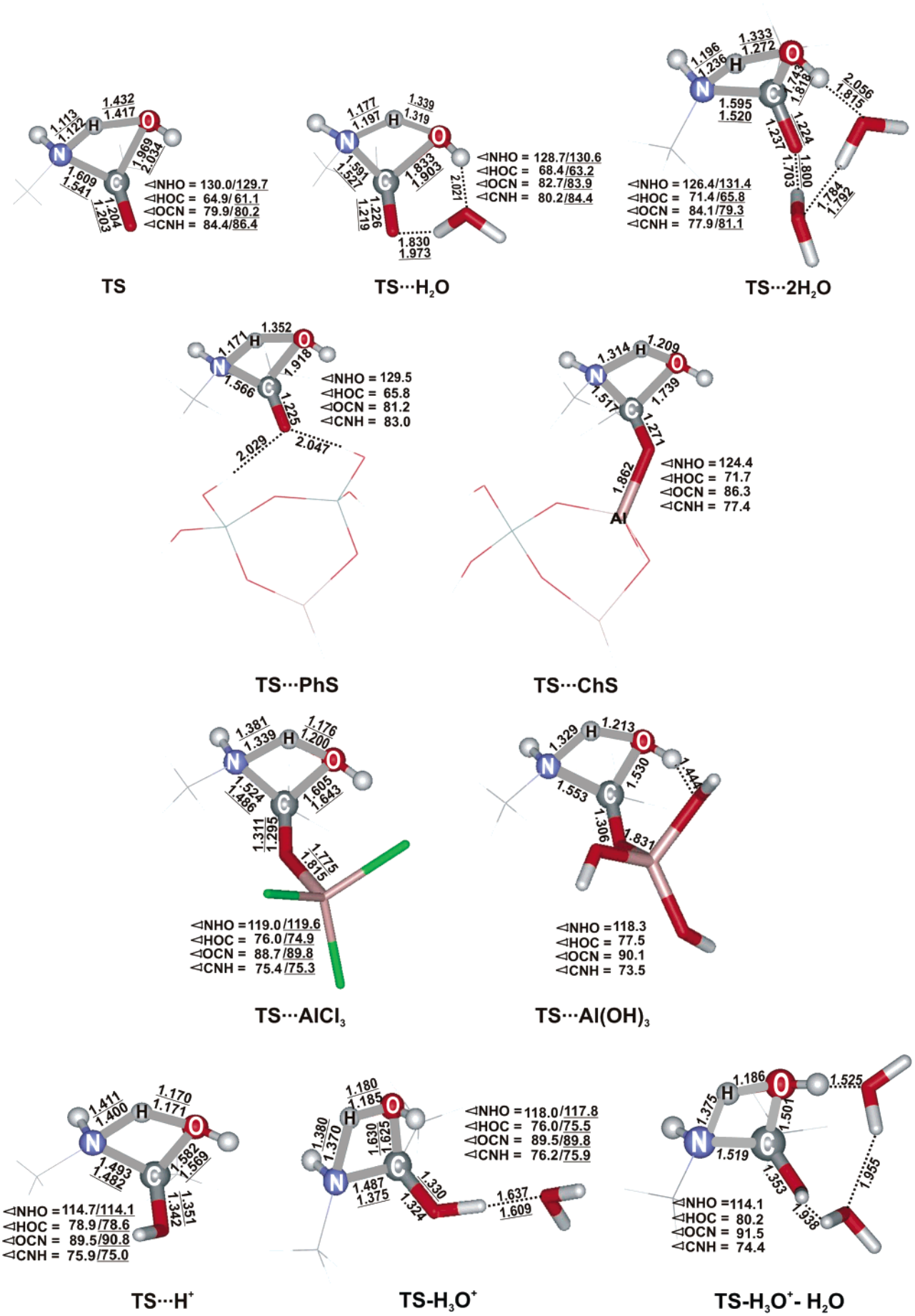

Figure 2. Saddle-point structures and most interesting geometric parameters. Underlined numbers refer to PCM results.

TABLE 4: Calculated Formation Energies of Pre-reaction Complexes ΔE_c, Activation Energies $\Delta E^{\#}_{fw}$, Overall Activation Energies $\Delta E^{\#}_{of}$, and Corresponding Thermodynamic Quantities Computed at the B3LYP/TZVP Level of Theory. The Last Column Contains Overall Solvent Activation Energies. All Energies Are in kcal/mol

	gas phase									
	complexation			activation			overall activation			solvent
model	ΔE_c	ΔH_c	ΔG_c	$\Delta E^{\#}_{fw}$	$\Delta H^{\#}_{fw}$	$\Delta G^{\#}_{fw}$	$\Delta E^{\#}_{of}$	$\Delta H^{\#}_{of}$	$\Delta G^{\#}_{of}$	$\Delta E^{\#}_{of}$
TS	−2.5	−1.0	7.1	41.2	38.2	42.9	38.7	37.2	50.0	36.5
TS···H_2O	−2.7	−1.4	6.5	43.5	40.4	44.9	40.8	39.0	51.4	38.2
TS···$2H_2O$	−2.7	−0.6	6.1	44.9	41.1	47.6	42.2	40.5	53.7	39.9
TS···PhS[a]	−5.8	–	–	45.6	–	–	39.8	–	–	33.0[b]
TS···ChS[a]	−7.0	–	–	37.8	–	–	30.8	–	–	32.7[b]
TS···$AlCl_3$	−6.3	−4.1	4.0	35.2	32.3	36.5	28.9	28.2	40.5	22.6
TS···$Al(OH)_3$	−6.8	−5.3	3.5	27.5	23.9	29.8	20.7	18.6	33.3	25.5
TS···H^+	−31.1	−28.1	−15.1	38.0	33.9	34.2	6.9	5.8	19.1	23.0
TS···H_3O^+	−16.8	−13.4	−0.7	32.9	28.8	29.2	16.1	15.4	28.5	23.5[b]
TS···(H_3O^+−H_2O)	−12.6	−9.0	4.4	32.4	28.2	28.5	19.8	19.2	32.9	25.3[b]

[a] Thermochemical data not calculated due to partial geometry optimization. [b] Single-point calculations at the gas-phase geometry.

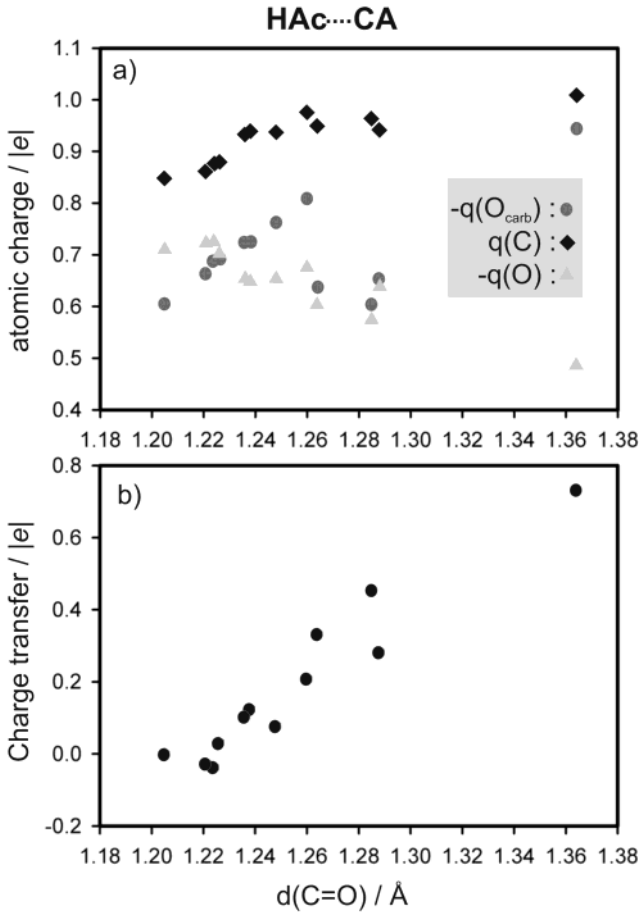

Figure 3. (a) NPA atomic charges of the C, O, O_{carb} atoms for the HAc···CA complexes in dependence on the C═O bond length, and (b) dependence of the total charge transfer between HAc and CA on the C═O bond length.

about 3.0 Å and fully optimizing these structures. The stationary points found in this way are not necessarily global minima, especially in the case of molecular complexes where water molecules are involved. However, the computed structures are directly connected to the transition state. Results are summarized in Table 4. We also have to note that calculated interaction energies are not corrected for the basis set superposition error (BSSE). Our previous experience with molecular complexes[38] allows us to estimate this correction to be approximately 1−2 kcal/mol.

The interaction energies for the first three systems given in Table 4 indicate the formation of weak complexes. In these structures the distances between the reaction centers N and C are about 3.8 Å. The reaction center of the nucleophile, the nitrogen atom, is not involved in any hydrogen bonds with other partners and, thus, is "free" to interact directly with the electrophile. Owing to entropic effects the complexation Gibbs free energies are positive, indicating that these complexes are thermodynamically unstable and will not exist in the pre-reaction phase.

Optimization of the pre-reaction complex in the presence of the physical surface (PhS) led to formation of hydrogen bonds not only between the carbonyl oxygen atom and the free surface hydroxyl group but also between the nitrogen atom of the MA molecule and the second free surface OH. The structure equilibrated at a N−C distance of about 4.3 Å and a complexation energy of −5.7 kcal/mol. Although the nitrogen atom is involved in the hydrogen bond formation and, thus, is partially blocked, the sterical arrangement of the whole complex allows a straightforward approach of both reaction centers. Thermodynamic quantities were not calculated in this case since only a partial geometry optimization was performed.

The presence of the second group of catalysts (strong Lewis acids ChS, $AlCl_3$, $Al(OH)_3$) changes the situation with the formation of the pre-reaction complex with the MA molecule. The strong activation of the HAc molecule (as it was discussed above) allows closer approach of the nucleophilic center to the carboxyl group. The N−C distances significantly decrease to values of about 3.0 Å. Moreover, hydrogen bond formation between one hydrogen atom of the $-NH_2$ group and the catalysts was observed. This means that also the $-NH_2$ group can be activated by the catalysts, which contain Lewis base sites (O and Cl atoms in our cases). These findings demonstrate the importance of both Lewis acid and base sites in the amide bond formation. The complexation energies for all three models are larger (in absolute value) than for the four previous cases. The complexation Gibbs free energies are still positive but closer to zero. Due to possible errors in the calculation of molecular entropy components in the harmonic-oscillator/rigid-rotor approximation, it is difficult to decide in these cases about the actual thermodynamic stability of these complexes.

The situation is different in the case of the charged catalysts H^+, H_3O^+, and $H_3O^+(H_2O)$. The extreme polarization of the HAc molecule and the large charge deficiency on the C_{carb} atom cause the formation of stable reaction intermediates with N−C distances of about 1.6 Å and high stabilization energies. The entropy factor reduces the stabilization energies, but for the

TABLE 5: NPA Charges for the C−O−H−N Reaction Center of the Transition State and for the Carbonyl Oxygen, and the Total Charge Transfer, CT, to the Catalyst[a]

model	q(C)	$-q(O_{OH})$	$-q$(OH)	q(H)	$-q$(N)	$-q(O_{carb})$	CT
TS	0.711	0.997	0.545	0.473	0.644	0.602	0.000
TS···H_2O	0.766	0.915	0.429	0.505	0.763	0.726	0.0047
TS···$2H_2O$	0.782	0.896	0.390	0.510	0.772	0.765	0.0015
TS···PhS							
TS···ChS	0.736	0.793	0.304	0.483	0.651	0.796	0.1631
TS···$AlCl_3$	0.687	0.751	0.234	0.495	0.637	0.853	0.1388
TS···$Al(OH)_3$	0.641	0.742	0.224	0.487	0.645	0.856	0.0632
TS···H^+	0.650	0.706	0.177	0.515	0.636	0.624	0.4859
TS···H_3O^+	0.663	0.717	0.204	0.505	0.629	0.669	0.4154
TS···(H_3O^+−H_2O)	0.635	0.705	0.173	0.506	0.637	0.671	0.3897

[a] Charges are in $|e|$.

complex with H^+ the Gibbs free energy is unambiguously negative. In the other two cases, the situation concerning ΔG_c is similar to the strong Lewis acids models. The activation energies presented in Table 4 also will be discussed later.

3.4. The Saddle-Point Structures for Amide-Bond Formation. The saddle-point structures are depicted in Figure 2, and the most interesting geometric parameters are given for each structure directly there. With the exception of two cases, the saddle points were assigned by a vibrational mode analysis to a proton transfer from the nitrogen atom to the hydroxyl group of the HAc molecule. The first exception refers to TS···[Al-$(H_2O)_5]^{3+}$. During the saddle-point search a regular C−N bond with the length of 1.520 Å was formed. The proton remained attached to the nitrogen atom. The hydroxylate group was abstracted from the −COOH group and combined with one proton from the closest water ligand of the pentaaqua aluminum, forming a water molecule. The new structure is no longer a transition state for the amide bond formation. The second exception is the TS···Al^{3+} complex. The saddle-point optimization procedure spontaneously led to the NMA molecule bound to the Al^{3+} cation via the C═O group and to a released water molecule. This situation is consistent with the strong exothermicity of the reaction HAc···Al^{3+} + MeA → NMA···Al^{3+} + H_2O (see Table 1). The two just-described exceptions were excluded from the tables related to transition states.

The structure of the reaction center in the isolated TS is similar to the structure of the transition state (TS3) of the NH_3 + HCOOH reaction reported in the investigations of Jensen et al.[21] and of Chalmet et al.[22] Following the interpretation of these authors, one finds that the amide bond formation proceeds in an asynchronous way. The CN bond is already formed to a large extent in TS, while the C−O(H) bond is strongly stretched by about 0.5 Å, leading to a weakly bound OH^- subunit with a charge of −0.545 $|e|$. The proton is still much closer to the nitrogen atom than to oxygen. Internal reaction coordinate (IRC) investigations (see also below) demonstrated that a major amount of the activation energy is needed for the proton transfer from the quarternary nitrogen to the OH^- subunit. Moreover, the C═O distance is significantly stretched by 0.05 Å as compared to the isolated HAc molecule.

The effect of the catalysts in the TS is similar to those effects observed for the original HAc···CA cases. The polarization of the C═O bond and its length increase in direct proportion to the strength of the catalyst. In all TS···CA saddle-point structures, the CN bond is already formed (see Figure 2). CN bond distances are smaller by a few hundredths of an Å in comparison to the uncatalyzed case for the weaker interactions and decrease up to 0.15 Å for TS···H_3O^+. The C−OH bond length is decreased significantly in all cases. It is interesting to observe that even for the weak interaction with one water molecule (TS···H_2O) a reduction of the C−OH bond length of 0.14 Å is found. It should already be noted here (for more details see below) that the global solvation effect is to stretch the C−OH bond again. The position of the migrating proton is also affected strongly in the TS···H_2O complex. It is almost amidst nitrogen and oxygen. Thus, even though the energy barrier is affected very little by the water molecule (see below), the geometry changes are substantial. Similar geometry changes in comparison to the isolated TS structure are found for the complexes TS···$(H_2O)_2$ and TS···PhS. Interaction of TS with the Lewis acids leads to a situation where the proton is already transferred to a large extent to the oxygen atom. Similar or even stronger effects are found for the charged catalysts. In total, the polarization of the C═O bond leads to a more compact structure by stabilizing the C−OH bond facilitating in this way the proton transfer.

In the cases where the PCM saddle-point optimizations were successful (TS, TS···H_2O, TS···$(H_2O)_2$, TS···$AlCl_3$, TS···H^+, and TS···H_3O^+) the most important structural parameters are given in Figure 2 as underlined numbers. For TS the effect of the continuum solvation model is to decrease the CN bond lengths in all cases. The C−OH bond length is increased for all neutral catalysts, i.e., the dissociation of the OH^- group is enhanced by PCM. Quite generally, for the complexes TS···H^+ and TS···H_3O^+, the changes in the structure of the reaction center are only slightly affected by PCM due to its compactness. For weak catalysts the NH bond is slightly contracted under the solvent effect, and for strong catalysts the NH bond is stretched. The changes of the OH distance are opposite to the changes of the NH distances since both are coupled via the same hydrogen atom. The observed trends show that the asynchronicity of the reaction (i.e., formation of the CN bond first, followed by proton transfer and H_2O abstraction) is enhanced by solvation for the weak catalysts. The same observations have been made by Chalmet et al.[22] It has already been mentioned above that the specific effect of water molecules explicitly included in the calculation (TS···H_2O and TS···$(H_2O)_2$) on the N−H and C−OH distances is opposite to the influence of global solvation. The combined effect computed in the semi-continuum calculations (PCM calculation for TS···H_2O) still shows a significant influence of the specific solvation effects. The situation is different in cases of the interaction with strong catalysts. The NH bond is stretched by global solvation shifting the saddle-point structure even closer to the product side.

A major difference between the NPA charges of HAc and TS (compare Tables 3 and 5) is the strong increase of the negative charge on O_{OH} in TS. A similar effect can be observed for the charges of the hydroxyl groups in HAc and TS. In combination with the already discussed strong elongation of the C−OH bond, this fact characterizes the situation as a hydroxide ion interacting with N-protonated NMA. For more details

concerning chemical bonding in the uncatalyzed reaction we refer to the extensive discussions given in refs 21 and 25. Under the effect of the catalysts, the charge distribution in the reaction center undergoes pronounced changes. The charge $q(O_{carb})$ increases (in absolute value) in proportion to the strength of the catalyst as was found for the interaction HAc···CA (the only exceptions are again the TS models H^+, H_3O^+, and $H_3O^+\cdots H_2O$). Only a moderate increase of the carbon charge and practically no change of the nitrogen charge are found. On the other hand, the polarization of the C═O bond by the catalyst stabilizes the C−OH bond (see the reduction of the C−O distances given in Figure 2), which results in a significant decrease of the charge (in absolute value) on O_{OH} and on the entire hydroxyl group (Table 5). This reduction is the consequence of the charge deficit on the carbon atom of the reaction center under the effect of the catalyst. The charge density is moved along the chain HO−C═O toward the catalyst. As expected, the largest total charge transfer to the catalyst was observed for the charged species, while the smallest one was found for water. It is interesting to note that also in the case of weak catalysts (water molecules, PhS) the charge transfer is directed from TS to the catalysts, in contrast to the situation found for the HAc···CA complexes. The TS structure adsorbed on the chemical clay surface (ChS) transfers to the catalyst a relatively large amount of the charge (0.14 $|e|$) similar to $AlCl_3$. The smaller total charge transfer to $Al(OH)_3$ is caused by back charge transfer from the $Al(OH)_3$ to the TS via the hydrogen bond formed between the OH group of the transition state and one oxygen atom of the $Al(OH)_3$. The same effect is also responsible for smaller charge transfer from the HAc molecule interacting with the $Al(OH)_3$ (see Table 3).

3.5. Reaction and Activation Energies. Reaction energies and thermodynamic data are presented in Table 1 for all studied reactions as far as available. To our knowledge, even for the uncatalyzed reaction experimental reaction enthalpies are not available. However, a reaction enthalpy of -0.4 ± 0.9 kcal/mol was calculated for the reaction between acetic acid and ammonia using experimental standard heats of formation.[54] This value agrees well with our calculated value of -0.9 kcal/mol (see Table 1). Differences between enthalpies and Gibbs free energies are small in all examples, thus indicating that any entropy effects in these reactions are not important. In the case of physical adsorption, the effect of the interaction with the catalyst on the reaction energy is not large. Significant relative stabilization of NMA in comparison to HAc is observed for chemical adsorption. This effect is particularly large for the charged catalysts.

Activation energies, enthalpies, and Gibbs free energies $\Delta E^{\#}_{fw}$ computed with respect to the pre-reaction complex $T^{\pm}\cdots$CA (eq 1) and $\Delta E^{\#}_{of}$ (eq 4) for the overall reaction are collected in Table 4. The amount of energy available for surmounting the activation barrier will depend on the details of the energy redistribution in the pre-reaction complex and on dissipation loss of energy to the surrounding medium. We have seen before that at the level of Gibbs free energies—with the exception of TS···H^+—the pre-reactive complex is not stable or only slightly stabilized and the dissipation losses should be limited. As will be seen just below, the results obtained for the two alternatives $\Delta G^{\#}_{fw}$ and $\Delta G^{\#}_{of}$ differ only by a few kcal/mol, excepting again the case TS···H^+. The true situation will probably be bracketed by these two ΔG values.

The barrier height $\Delta E^{\#}_{of}$ is practically not affected by the relatively weak, hydrogen-bonded interactions. The chemical surface defects ChS, $AlCl_3$, and $Al(OH)_3$ show significant reductions of the barrier height by up to 25 kcal/mol. Protonation reduces the barrier drastically. The more realistic protonation models for solution, H_3O^+ and $H_3O^+-H_2O$, give barrier heights of about 16−20 kcal/mol. A comparison of $\Delta H^{\#}_{of}$ and $\Delta G^{\#}_{of}$ values given in Table 4 shows that entropy effects are very important for the formation of the activated complex. The difference is about 13 kcal/mol, which is practically the same for all catalysts. Similar results have been reported by Oie et al.[18] and Jensen et al.[21] The variation of the barrier heights $\Delta E^{\#}_{fw}$ is much less pronounced than the one for $\Delta E^{\#}_{of}$ since a strong stabilization of the transition complex also means a strong stabilization of the pre-reactive complex. Nevertheless, significant reductions of the barrier heights are found for $\Delta E^{\#}_{fw}$ as well. At the level of $\Delta G^{\#}_{fw}$, all strongly interacting systems show a reduction with respect to the uncatalyzed case by about 7−10 kcal/mol.

Solvation effects reduce the overall activation barrier for the uncatalyzed reaction and of the physically adsorbed catalysts by a few kcal/mol. In the other cases the barrier is increased, in some cases quite substantially. The reason for this increase is that solvation of the separated reactants is more favorable than of the activated complex because of the larger solvent-accessible surface in the former case. For a discussion of these global solvation effects see also ref 55. However, as one knows from the investigations of Oie et al.[19] and Antonczak et al.,[23] specific catalytic effects of water or ammonia are significant and will reduce the barrier again.

In addition to the verification of the transition states by a normal-mode analysis IRC calculations were performed. Results for three selected cases (TS, TS···$AlCl_3$, and TS···H^+) in the gas phase are shown in Figure 4. All energy profiles are given in relation to the respective saddle-point energies. The evolution of the interatomic distances with the reaction coordinate shows that the CN bond is practically formed when the proton-transfer begins. This happens in all cases at about $R_c = -1.5$. This is in very good agreement with the findings of Chalmet et al.[22] However, the subsequent proton transfer proceeds in a different way for the uncatalyzed TS and for the interactions with the strong catalysts. In the latter cases the increase of the NH bond and the decrease of the OH bond are much steeper than for TS alone. It should also be noted that the behavior of the interatomic distances is similar for TS···$AlCl_3$ and TS···H^+. As we saw already in the discussion of the saddle-point structures, the NH and OH bonds are practically equidistant in these two cases, whereas for TS alone the crossing between the curves for the NH and OH bonds occurs distinctively later. The analysis of the energy profiles shows that the main energetic contribution to the reaction barrier is connected with the proton transfer. The best example confirming this fact is the TS···H^+ model and its activation energy $\Delta E^{\#}_{fw}$ given in Table 4. We discussed above that, in this case, a stable pre-reaction complex with the N−C bond of 1.573 Å is formed. Thus, practically the whole energy necessary to activate the transition state is spent for the proton transfer between the N and O atoms.

Chalmet et al.[22] showed that for the uncatalyzed reaction the evolution of the NH and OH bonds is practically identical for continuum solvation and gas phase. Thus, continuum solvation does not have any remarkable influence on the energetic (see above) and structural course of the reaction in this case. In contrast thereto, the specific solvation by one or two water molecules has a significant influence on the reaction profile. Analysis of the evolution of the proton transfer (not given in Figure 4) shows an increase/decrease of the NH/OH bonds between the uncatalyzed and the TS···$AlCl_3$ cases. The impor-

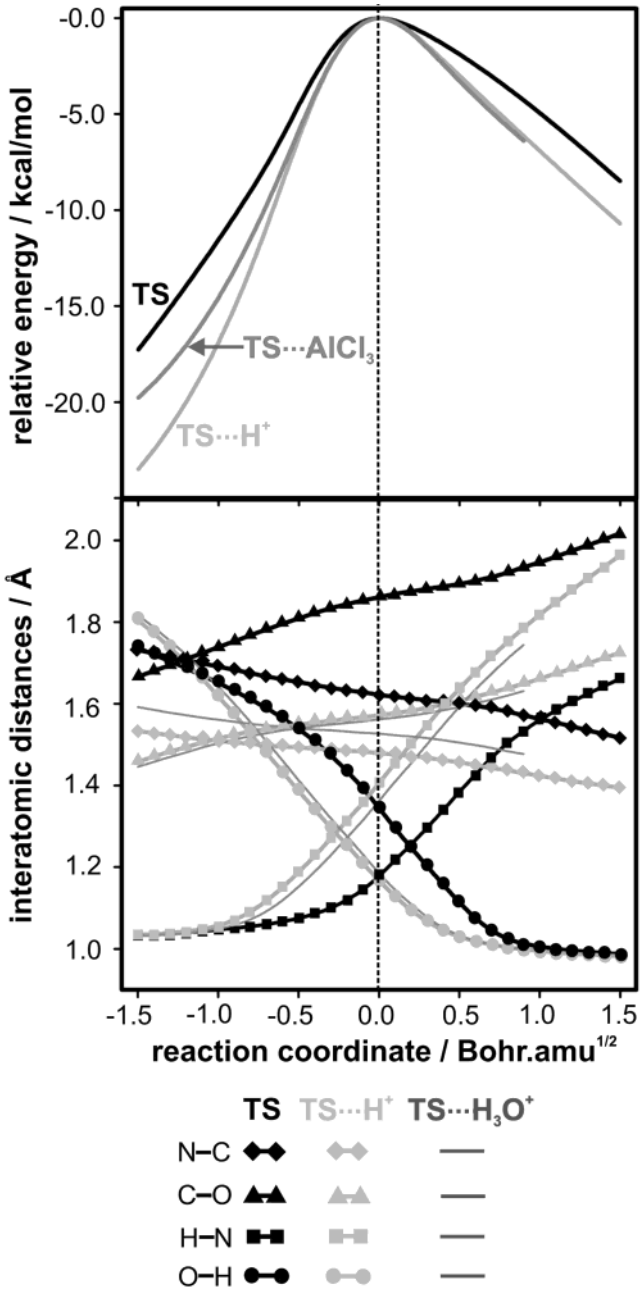

Figure 4. Variation of the energy and selected interatomic distances in the reaction center along the reaction coordinate for the TS, TS···$AlCl_3$, and TS···H^+ systems. The energies are given relative to the saddle-point energy.

tance of hydrogen bonding to the carbonyl group for reactive trajectories has been observed also in the QM/MM molecular dynamics calculations of Chalmet at al.[22]

IV. Conclusions

The effect of the C═O bond polarization on the amide bond formation between acetic acid and methylamine has been investigated using a series of catalysts of increasing strength. Only the one-step mechanism has been treated in this work. Similar results concerning the effect of the C═O bond polarization are expected for the two-step mechanism. In all cases, even in those of strong polarization of the C═O bond, an asynchronous reaction path was observed on the basis of an IRC analysis. The question of stable pre-reaction molecular complexes under the effect of catalysts was investigated too. In the first phase of the reaction, the CN bond is formed as it has already been described for the uncatalyzed reaction.[21,22] In the second phase, the proton transfer from nitrogen to the oxygen (O_{OH}) is taking place. This second step is strongly influenced by the catalyst in facilitating the proton transfer. The catalysts can be divided into three groups according to their ability to decrease the activation barrier for the amide bond formation. The first group contains neutral compounds (water molecules and the physical clay surface defect) forming standard hydrogen bonds. This group has only a small effect on the energy barrier. However, the course of the proton transfer is affected significantly in the sense that it occurs earlier as compared to the uncatalyzed system. In contrast thereto, the continuum solvation model shows only a small effect. This example demonstrates that the explicit inclusion of water molecules in solvation models is important and the four reacting centers show significant structural flexibility even in the case of the relatively weak, hydrogen-bonded interactions. For this group of catalysts no thermodynamically stable pre-reaction complex was found. Thus, differences between the activation and overall activation energies are small.

The second group of catalysts contains the Lewis acids ($AlCl_3$, $Al(OH)_3$, and the chemical clay surface defect). $Al(OH)_3$ interacts also via hydrogen bonds to its OH groups. The pre-reaction complexes are energetically more stable than in the first group of catalysts. This fact is reflected in higher differences between the activation and overall activation energies. Nevertheless, generally a strong reduction of the energy barrier and of the proton-transfer process was observed. The third group contained charged catalysts (H^+, H_3O^+, $H_3O^+-H_2O$, Al^{3+}, and $Al(H_2O)_5^{3+}$). As was expected because of the 3-fold positive charge, the last two examples had the strongest influence, resulting in different reaction mechanisms. In these latter two cases, no saddle points have been observed. The three other examples showed that protonation is very effective in reducing the energy barrier for amide bond formation. The same observation has already been made by Antonczak et al.[23] in the context of the reverse process of amide bond hydrolysis. For the stable pre-reaction complexes with high complexation energies, the first phase of the reaction (nucleophillic attack of N on C) is practically completed since N−C distances of about 1.6 Å are observed. The strong complexation produces relatively large differences between the activation and overall activation energies. Although overall activation energies are apparently lower with respect to the other cases, calculated activation energies related to the pre-reaction complexes are similar to activation energies obtained for the neutral Lewis acids. However, at the ΔG level, differences between activation and overall activation energies are not so pronounced anymore. Generally, the strong Lewis acid sites significantly facilitate the nucleophilic attack and as dominant bottleneck for the reaction remains the proton transfer.

Conclusions with respect to the role of mineral surfaces on the catalysis of the amide bond formation are as follows. Surfaces covered with hydroxyl groups such as, e.g., in kaolinite, provide only normal hydrogen-bonded interactions. The reaction activity of such surfaces is similar to our first group of weak catalysts and will not be very effective to promote the amide bond formation. More active defects such as unsaturated (Lewis acid) aluminum defects, as investigated in this work, or eventually other defects such as OH_2^+ or O^-, are required for efficient enhancement of amide-bond formation. Solvated Al^{3+} and other similar cations can also be extremely efficient. This agrees with experimental observations,[9−14] where, for example, clay minerals with a high concentration of the surface defects

(e.g., montmorillonites) and/or γ-alumina, respectively, were evaluated as good catalysts. It is clear that various factors will have to be considered in these catalyzed reactions. For example, the interaction of a Lewis acid defect with solvent molecules can reduce its possible assistance in the reaction, resulting in a reduction of catalytic efficiency. Thus, tuning of reaction conditions such as pH and concentration of Lewis acid sites seems to be very important, and the inclusion of these factors into computational models represents a challenge for future studies.

Acknowledgment. This work was supported by the Austrian Science Fund, Project No. P15051-CHE. We are grateful for technical support and computer time at the Linux-PC cluster Schrödinger II of the computer center of the University of Vienna.

Supporting Information Available: Total energies and Cartesian geometries for all structures investigated in this work computed at the B3LYP/TZVP level in the gas phase. This material is available free of charge via the Internet at http://pubs.acs.org.

References and Notes

(1) Bernal, J. D. *The Physical Basis of Life*; Routledge and Kegan Paul: London, 1951; p 34.
(2) Lawles, J. G. *Clay-organic interactions and the origin of life*. In *Clay minerals and the origin of life*; Cairn-Smith, A. G., Hartman, H., Eds.; Cambridge University Press: Cambridge, 1988; p 135.
(3) Theng, B. K. G. *Organic reactions catalyzed by clay minerals*. In *The chemistry of clay-organic reactions*; Bristol: Hilger, 1974; p 261.
(4) Yamada, S.; Terashima, S.; Wagatsuma, M. *Tetrahedron Lett*. **1970**, 1501.
(5) Plankensteiner, K.; Righi, A.; Rode, B. M. *Origins Life Evol. Biosphere* **2002**, *32*, 225.
(6) Rode, B. M. *Peptides* **1999**, *20*, 773.
(7) Bujdák, J.; Rode, B. M. *Geologica Carphatica − Series Clays* **1995**, *4*, 37.
(8) Kessaissia, S.; Siffert, B.; Donnet, J. B. *Clay Miner*. **1980**, *15*, 383.
(9) Bujdák, J.; Rode, B. M. *J. Mol. Evol*. **1996**, *43*, 326.
(10) Bujdák, J.; Rode, B. M. *J. Mol. Catal. A* **1999**, *144*, 129.
(11) Bujdák, J.; Rode, B. M. *Origins Life Evol. Biosphere* **1999**, *29*, 451.
(12) Bujdák, J.; Rode, B. M. *Amino Acids* **2001**, *21*, 281.
(13) Basiuk, V. A.; Sainz-Rojas, J. *Adv. Space Res.* **2001**, *27*, 225.
(14) Bujdák, J.; Rode, B. M. *J. Inorg. Biochem*. **2002**, *90*, 1.
(15) Gresser, M. J.; Jencks, W. P. *J. Am. Chem. Soc*. **1977**, *99*, 6970.
(16) Cox, M. M.; Jencks, W. P. *J. Am. Chem. Soc.* **1981**, *103*, 572.
(17) Yang, C. C.; Jencks, W. P. *J. Am. Chem. Soc*. **1988**, *110*, 2972.
(18) Oie, T.; Loew, G. H.; Burt, S. K.; Binkley, J. S.; MacElroy, R. D. *J. Am. Chem. Soc*. **1982**, *104*, 6169.
(19) Oie, T.; Loew, G. H.; Burt, S. K.; MacElroy, R. D. *J. Am. Chem. Soc*. **1983**, *105*, 2221.
(20) Oie, T.; Loew, G. H.; Burt, S. K.; MacElroy, R. D. *J. Am. Chem. Soc*. **1984**, *106*, 8007.
(21) Jensen, J. H.; Baldridge, K. K.; Gordon, M. S. *J. Phys. Chem*. **1992**, *96*, 8340.
(22) Chalmet, S.; Harb, W.; Ruiz-López, M. F. *J. Phys. Chem. A* **2001**, *105*, 11574.
(23) Antonczak, S.; Ruiz-López, M. F.; Rivail, J. L. *J. Am. Chem. Soc*. **1994**, *116*, 3912.
(24) Bakowies, D.; Kollman, P. A. *J. Am. Chem. Soc*. **1999**, *121*, 5712.
(25) Krug, J. P.; Popelier, P. L. A.; Bader, R. F. W. *J. Phys. Chem*. **1992**, *96*, 7604.
(26) Remko, M.; Rode, B. M. *Phys. Chem. Chem. Phys*. **2001**, *3*, 4667.
(27) Ward, D. B.; Brady, P. B. *Clays Clay Miner*. **1998**, *46*, 453.
(28) Tunega, D.; Benco, L.; Haberhauer, G.; Gerzabek, M.; Lischka, H. *J. Phys. Chem. B* **2002**, *106*, 11515.
(29) Tunega, D.; Haberhauer, G.; Gerzabek, M.; Lischka, H. *Soil Sci*., accepted.
(30) Car, R.; Parinello, M. *Phys. Rev. Lett.* **1985**, *55*, 2471.
(31) Kresse, G.; Hafner, J. *Phys. Rev. B* **1993**, *48*, 13115.
(32) Kresse, G.; Furthmülleer, J. *J. Comput. Mater. Sci*. **1996**, *6*, 15.
(33) Chatterjee, A.; Iwasaki, T.; Ebina, T. *J. Phys. Chem. A* **2000**, *104*, 2098.
(34) Kubicki, J. D.; Blake, G. A.; Apitz, S. E. *Geochim. Cosmochim. Acta* **1997**, *61*, 1031.
(35) Gorb, L.; Gu, J.; Leszczynska, D.; Leszczynski, J. *Phys. Chem. Chem. Phys*. **2000**, *2*, 5007.
(36) Pelmenschikov, A.; Leszczynski, J. *J. Phys. Chem. B* **1999**, *103*, 6886.
(37) Tunega, D.; Haberhauer, G.; Gerzabek, M.; Lischka, H. *Langmuir* **2002**, *18*, 139.
(38) Aquino, A. J. A.; Tunega, D.; Haberhauer, G.; Gerzabek, M. H.; Lischka, H. *J.* Comput. Chem. **2003**, *24*, 1853.
(39) Hay, R. W.; Porter, L. J. *J. Chem. Soc*. **1967**, 1261.
(40) Frisch, M. J.; Trucks, G. W.; Schlegel, H. B.; Scuseria, G. E.; Robb, M. A.; Cheeseman, J. R.; Zakrzewski, V. G.; Momtegomery, J. A., Jr.; Stratmann, R. E.; Burant, J. C.; Dapprich, S.; Millam, V.; Daniels, A. D.; Kudin, K. N.; Strain, M. C.; Farkas, O.; Tomasi, J.; Barone, V.; Cossi, M.; Cammi, R.; Mennucci, C.; Pomelli, C.; Adamo, S.; Clifford, J.; Ochterski, G. A.; Petersson, P. Y.; Ayala, B.; Cui, Q.; Morokuma, K.; Malick, D. K.; Rabuck, A. D.; Raghavachari, K.; Foresman, J. B.; Cioslowski, J.; Ortiz, J. V.; Stefanov, B. B.; Liu, G.; Liashenko, A.; Piskorz, P.; Komaroni, I.; Gomperts, R.; Martin, R. L.; Fox, D. J.; Keith, T.; Al-Laham, M. A.; Peng, C. Y.; Nanayakkara, A.; Gonzalez, C.; Challacombe, M.; Gill, P. M. W.; Johnson, B.; Chen, W.; Wong, M. W.; Andres, J. L.; Head-Gordon, M.; Reploge, E. S.; Pople, J. A. *Gaussian98, Revision A.11*; Gaussian, Inc.: Pittsburgh, PA, 1998.
(41) Becke, A. D. *J. Chem. Phys*. **1993**, *98*, 5648.
(42) Schäfer, A.; Huber, C.; Ahlrichs, R. *J. Chem. Phys.* **1994**, *100*, 5829.
(43) Gonzales, G.; Schlegel, H. B. *J. Chem. Phys*. **1989**, *90*, 2154.
(44) Gonzales, G.; Schlegel, H. B. *J. Chem. Phys*. **1990**, *94*, 5523.
(45) Reed, A. E.; Weinstock, R. B.; Weinhold, F. *J. Chem. Phys*. **1985**, *83*, 735.
(46) Head-Gordon, M.; Pople, J. A.; Frisch, M. J. *Chem. Phys. Lett*. **1988**, *153*, 503.
(47) Frisch, M. J.; Head-Gordon, M.; Pople, J. A. *Chem. Phys. Lett*. **1990**, *166*, 275.
(48) Frisch, M. J.; Head-Gordon, M.; Pople, J. A. *Chem. Phys. Lett*. **1990**, *166*, 281.
(49) Schäfer, A.; Horn, H.; Ahlrichs, R. *J. Chem. Phys*. **1992**, *97*, 2571.
(50) Miertus, S.; Scrocco, E.; Tomasi, J. *Chem. Phys*. **1981**, *55*, 117.
(51) Miertus, S.; Tomasi, J. *Chem. Phys.* **1982**, *65*, 239.
(52) Cossi, M.; Barone, V.; Cammi, R.; Tomasi, J. *Chem. Phys. Lett*. **1996**, *255*, 327.
(53) Kubicki, J. D.; Schroeter, L. M.; Itoh, M. J.; Nguyen, B. N.; Apitz, S. E. *Geochim. Cosmochim. Acta* **1999**, *63*, 2709.
(54) Dobbs, K. D.; Dixon, D. A. *J. Phys. Chem*. **1996**, *100*, 3965.
(55) Aquino, A. J. A.; Tunega, D.; Haberhauer, G.; Gerzabek, M. H.; Lischka, H. *J. Phys. Chem. A* **2002**, *106*, 1862.